EIC Calorimetry

Introduction

The general idea of calorimetry is to measure the energy of a particle as it passes through the detector. It is designed to stop or absorb most of the particles coming from a collision. Calorimeters consist of absorbing high-density material. Electromagnetic calorimeters measure the energy of electrons and photons as they interact with matter producing electromagnetic showers. The summed ionization is proportional and a good measure of the incident energy. Also important are position and time resolution. Hadronic calorimeters measure mainly hadrons as they interact with matter producing hadronic showers, which contain both an electromagnetic and a strong interaction component, e.g. fission, knock-off, delayed photons. The electromagnetic fraction increases with energy, which leads to nonlinearity. One of the important aspects in hadron calorimetry is thus the optimization of the electron to photon response ratio, the compensation condition.

EM Calorimetry

An electromagnetic shower is normally initiated by a high energetic photon or electron. When a photon of sufficient energy enters a detector material an electron-positron pair is produced with high probability. Both, the photon and the produced pair lose energy due to ionization of the surrounding medium and, if their energy exceeds the critical energy E_c of the material, in turn radiate by Bremsstrahlung and produce new high energetic photons. These again are converted into electrons or positrons, which leads to the development of a cascade of electromagnetic reactions, or shower. The shower development ends if the secondary photon energy is insufficient for pair production or the lepton energy is considerably smaller than E_c. A schematic view of the shower development is shown in Figure 1.

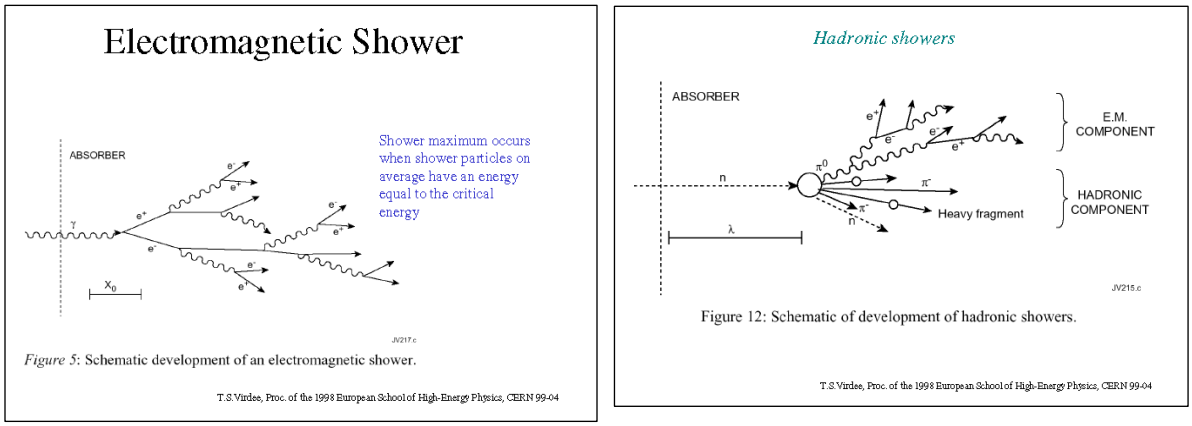

Fig. 1: schematic representation of an electromagnetic (left) and hadronic shower (right)

The propagation of an electromagnetic shower is divided into longitudinal development in the direction of the initial particle and into lateral or transversal development. The relevant quantities to describe the longitudinal shower are the energy of the initial particle and penetration depth into the detector medium. A rough approximation for the longitudinal energy containment of an electromagnetic shower is that 98% of the incoming particle energy is deposited in a depth equal to three times the shower center of gravity. The lateral spread of the electromagnetic shower is caused mainly by the angular distribution of Bremsstrahlung and the multiple scattering of electrons and positrons, but Compton scattering and photoelectric effect contribute as well and are even able to emit particles in backward direction. The mean transverse detection scales with the Molière radius (R_M) of the absorber material. The parametrization for the energy deposited in distance r from the shower axis depends on geometry and material budget of absorber or detector. Detectors are often laterally segmented which enables the determination of the point of impact of the incident particle. It is deduced from the energy distribution in the individual responding segments. Nevertheless, this segmentation also can also result in lateral energy leakage, which deteriorates the energy response. A width of a single segment of one R_M has been proven to represent a good compromise between lateral spatial sensitivity and a preferably complete energy containment.

A typical ElectroMagnetic (EM) calorimeter is a light-transparent, homogeneous, crystal calorimeter with dimensions large enough to contain the complete shower of secondary particles. Crystal calorimeters have been used in nuclear and high energy physics for their high resolution and detection efficiency. They do not provide longitudinal shower information. The readout of crystal calorimeters is mostly light-based, which tends to be in the blue range. The classical option is photomultiplier tubes, whose contribution to the noise level is negligible as one can cut on the single photoelectron. Advanced readout options include Avalanche Photo-Diodes and Silicon-Photo-multipliers. Homogeneous electromagnetic calorimeters have been used at, e.g. JLab ($PbWO_4$) [1], KTeV (CsI) [2,3], BaBar [4,5] and Belle (CsI(TI)) [6,7], CMS ($PbWO_4$) [8,9] and L3 (BGO) [10,11]. The latter two are complemented by hadronic calorimeters. Table 1 lists some of the properties of these systems.

Technology	**Experiment**	**Depth**	**Energy resolution**	**Readout**
NaI(TI)	Crystal Ball	$20X_0$	$2.7\%/E^{1/4}$	
$Bi_4Ge_3O_{12}$ (BGO)	L3	$22X_0$	$2\%/\sqrt{E} + 0.7\%$	
CsI	KTeV	$27X_0$	$2\%/\sqrt{E} + 0.45\%$	
CsI(TI)	BaBar	$16\text{-}18X_0$	$2.3\%/E^{1/4} + 1.4\%$	SiPM
CsI(TI)	Belle	$16X_0$	$2\%/\sqrt{E}$	SiPM
$PbWO_4$	CMS	$25X_0$	$3\%/\sqrt{E} + 0.5\% + 0.2/E$	APD
$PbWO_4$	Primex		$1.75\%/\sqrt{E} + 1.15\%$	PMT
$PbWO_4$	PANDA		$<2\%/\sqrt{E} + <1\%$ (req.)	LAAPD
$PbWO_4$	NPS		$<2\%/\sqrt{E} + <1\%$ (req.)	PMT

Lead glass	OPAL	$20.5X_0$	$5\%/\sqrt{E}$	
Liquid Kr	NA48	$27X_0$	$3.2\%/\sqrt{E} + 0.42\% + 0.09/E$	

Table 1: examples of homogeneous EM calorimeter systems based on crystals [1, 2, 4, 6, 8, 9, 12, PANDA,NPS], lead glass [13] or noble gas liquids [14,15].

One important aspect in electromagnetic calorimeter design is compactness coupled with high resolution, timing, and radiation hardness. The material of choice for recent experiments has been the inorganic scintillator lead tungstate ($PbWO_4$), which features a small Moliere radius (R_M=2.0 cm), high density (8.3 g/cm^3), fast response (<2ns), and radiation resistance. $PbWO_4$ has been used for existing calorimeters (CMS, JLab Hall B) and high quality crystals are being considered to be used in several new electromagnetic calorimeter projects around the world (PANDA, JLab 12 GeV). Energy resolutions of better than 2% for energies 0.05-15 GeV have been achieved with the PANDA prototype with a constant term of order 0.6-0.7%. CMS achieved a constant term of 0.3% albeit at higher energies (20-250 GeV). For comparison, the energy resolution of lead glass is 5-6%. The energy resolution of $PbWO_4$ can be further improved by cooling the crystals.

Most calorimeters in high energy physics are sampling calorimeters as the cost of homogenous crystal ones would be unaffordable. Sampling calorimeters consist of an active (readout, e.g. scintillator or Cherenkov radiator) and a passive (absorber, e.g. Pb, Cu, W) component. They provide high granularity in both lateral and longitudinal direction, but energy resolution is substantially lower than that of crystal calorimeters. The key parameter for this type of calorimeter is the sampling fraction, which is the ratio of energy resolution of active to the sum of active and passive layers. There are many ways to build sampling calorimeters, e.g. sandwich, spaghetti, etc. types, where the sandwich type has been most popular. Light collection (analog vs. digital) is an important consideration for sampling calorimeters as sampling fluctuations directly impact energy resolution. The most popular solutions are SPACAL (Pb, scintillating fibers) and sandwich with Wave-Length-Shifting (WLS) fibers crossing through ("Shashlik"). In both cases the fibers are bundled to the PMT. The timing resolution of these detectors is typically 50 ns limited by scintillation and photodetector time. Examples of sampling calorimeters are the SpaCal calorimeter at H1 at DESY, the barrel calorimeter in Hall D at JLab, the Shashlyk calorimeter for the KOPIO experiment at BNL and the calorimeter of the Collider Detector at Fermilab (CDF). The latter has a projective tower geometry with fine granularity and consists of seven sampling calorimeter systems. The central calorimeter has plastic scintillators as active volume while gas proportional chambers are used for the other systems. Typical energy resolutions of existing sampling calorimeters are $\sigma_E / E = 10\%/\sqrt{E} + 0.8\%$ compared to $\sigma_E / E = 2\%/\sqrt{E} + 0.3\%$ for crystal calorimeters.

Technology	**Exp.**	**Depth**	**EM Energy resolution**	**Readout**
Scintillator/depleted U	ZEUS	$20\text{-}30X_0$	$18\%/\sqrt{E}$	PMT

Scintillator/Pb	CDF	$18X_0$	13.5%/√E +2.5%	
Scintillator fiber/Pb spaghetti	KLOE	$15X_0$	5.7%/√E + 0.6%	PMT
Liquid Ar/Pb	NA31	$27X_0$	7.5%/√E + 0.5% + 0.1/E	
Liquid Ar/Pb	SLD	$21X_0$	8%/√E	
Liquid Ar/Pb	H1	$20\text{-}30X_0$	12%/√E + 1%	
Liquid Ar/depl. U	D0	$20.5X_0$	16%/√E + 0.3% + 0.3/E	
Liquid Ar/Pb accordion	ATLAS	$25X_0$	10%/√E + 0.4% + 0.3/E	
Scintillator/Pb	CLAS	$15X_0$	10%/√E	PMT
Scintillator/Pb	GluEx	$15X_0$		SiPM

Table 2: examples of sampling EM calorimeter systems based on layers of low X_0 passive material interleaved with active material based on plastic scintillators [16-19], gas [20, 22], silicon + dense materials (Fe, Pb, W, …). The energy resolution depends on sampling fluctuations.

Hadronic Calorimetry

Hadronic showers are more complex than electromagnetic showers. They include both, electromagnetic components from neutral pions and strong interaction components from, e.g. neutrons, protons and charged pions. The cross section for the hadron losing energy by nuclear reactions is low, but the energy loss is high. It is mainly caused by protons losing energy by ionization, neutral pions decaying into two photons starting electromagnetic showers, breaking up nuclei and neutrino production. A simple calculation of these processes is not possible, but Monte Carlo simulations can provide empirical results for the longitudinal and transverse shower development. The longitudinal shower development is expressed in terms of the interaction length, which contains most of the energy deposited. Nearly all the energy is deposited in about five interaction lengths. In general, hadronic showers are much broader and extend deeper into the detector than electromagnetic showers.

For hadron calorimetry, crystals would be impractically large. Hadronic calorimeters thus sample the energy of hadrons (particles that contain quarks, such as protons and neutrons) as they interact with atomic nuclei. The energy measurement of hadrons is incomplete due to the missing energy due to the invisible shower components, e.g. neutrinos from charged pion decay. This results in a lower calorimeter response to hadron showers compared to that to EM showers of the same energy. The ratio of calorimeter response to EM and hadronic components can be expressed as

$$e/h = \frac{e/h\,(non-EM)}{1-f_{EM}\left[1-e/h\,(non-EM)\right]}, \qquad (1)$$

where f_{EM} is the electromagnetic shower fraction. The performance of hadronic calorimeters is thus directly affected by fluctuations in f_{EM}. For homogeneous calorimeters, where the constituent material acts as absorber and as active material, a typical ratio is e/h=2. For sampling

calorimeters, where separate absorbing layers are interspersed with active material layers, the compensation can be achieved, i.e. *e/h*=1. The mechanism is to either suppress the electromagnetic response by higher Z absorbers or boost the response to non-electromagnetic components by, e.g. increasing the number of neutrons. The latter can be achieved by increasing the hydrogen concentration of the active material. Other methods to correct for the different calorimeter response to electromagnetic and hadronic components of the shower are discussed in the next paragraphs. Typical resolutions are worse than in EM calorimeters, e.g. $\sigma_E/E \sim (35\%-94\%)/E$.

There have been many ways to build hadronic calorimeters, e.g. sandwich style like CDF. Traditional methods rely on the combination of electromagnetic and hadron calorimeters to reconstruct the energy. In this case, 70% of the energy is measured in the hadron calorimeter with poor resolution. As an example, the energy resolution of the CMS hadronic calorimeter is $94\%/\sqrt{E}+4.4\%$. That resolution can be improved by using the full calorimetric system (ECAL+HCAL). The combined resolution of the CMS hadronic calorimeter is $83\%/\sqrt{E}+4.5\%$. Current efforts focus on dealing with the sampling fluctuations in EM and hadronic showers. These fluctuations are only a minor contribution to hadronic resolution in non-compensating calorimeters while EM resolution is dominated by sampling fluctuations. The ultimate limit of hadronic energy resolution are fluctuations in visible energy. The fluctuations in the EM shower fraction are also important.

To determine the requirement on the hadronic energy resolution, one has to evaluate the required energy resolution of the jets, which are produced particles boosted into the original direction of the quark. There are currently two methods that address jet energy resolution: 1) Particle Flow Algorithms (PFA) that minimize the influence of the hadronic calorimeter and measure jets using the combination of the whole detector, 2) Dual Readout (DREAM) that explores measurement of the hadronic shower components in each event and weight them accordingly to directly access the source of fluctuations. This would provide the ultimate energy jet resolution achievable.

The basic principle of the particle flow analysis is to choose the detector that is best suited to detect a particular particle type. For example, one measures charged particles in the tracker, photons in the EM calorimeter (typical resolutions $2\text{-}10\%/\sqrt{E}$) and neutral hadrons only in the hadron calorimeter. In this case only 10% of the jet energy is measured in the hadronic calorimeter resulting in much improved jet resolution. As an example, for a jet energy fraction on the order of 10% and particle resolutions on the order of $30\text{-}40\%/\sqrt{E}$ the jet energy resolution is on the order of $10\text{-}20\%/\sqrt{E}$(jet). Another method is the Dual-Readout approach in which one compares the relative strengths of the signals representing the visible deposited energy and the Cherenkov light produced in the shower absorption process, and reconstructs the EM shower fraction and total shower energy from the known *e/h* values of the calorimeter. In dual-readout calorimeters, signals are generated in scintillating fibers, which measure the deposited energy, and in clear plastic fibers, which measure the relativistic shower particles. A current effort with a

dual readout fiber calorimeter demonstrated reconstruction of the energies of proton and pion within a few percent at energies between 10 GeV and 180 GeV. The fractional widths of the signal distribution for these particles scale with beam energy as 30%/√E without additional contributing terms [23].

Technology	Exp.	Hadronic Energy resolution	Readout
Streamer tubes/Fe	ALEPH	85%/√E	PMT
Scintillator/depleted U	ZEUS	35%/√E +2%	PMT
Scintillator/brass	CMS	94%/√E+4.5%	HPD/SiPM
Scintillator/Fe	ATLAS	53%/√E+5.7	
Scintillator/Fe	CDF	(50-70)%/√E	
Scintillator/Fe	LHCb	69%/√E+9%	PMT
Liquid Ar/Fe	H1	51%/√E +1.6%+0.9/E	
Liquid Ar/U	D0	41%/√E +3.2%+1.4/E	

Table 3: examples of sampling hadronic calorimeter systems based on layers of low X_0 passive material interleaved with active material based on plastic scintillators, gas, silicon + dense materials (Fe, Pb, W, …). The energy resolution depends on sampling fluctuations. ZEUS [Derrick],

Calorimetry at the Electron Ion Collider - Overview

The physics program of an EIC includes inclusive measurements, which require detection of the scattered lepton and/or hadrons of the scattered hadronic debris for which E-p_z is different from zero; semi-inclusive processes, which require detection in coincidence with the scattered lepton of at least one (current or target region) hadron; and exclusive processes which require detection of all particles in the reaction with high precision [24-26]. For design and placement of calorimetry at an EIC, one has to pay attention to the requirements on particle identification and precision in reconstruction in different regions of the produced particles' angle and momentum distributions. As an example, precision in reconstruction directly impacts the resolution of the four-momentum transfer, t, of the hadronic system required for 3D imaging with exclusive reactions. The available space in each region and allowable material budget are also of considerable importance.

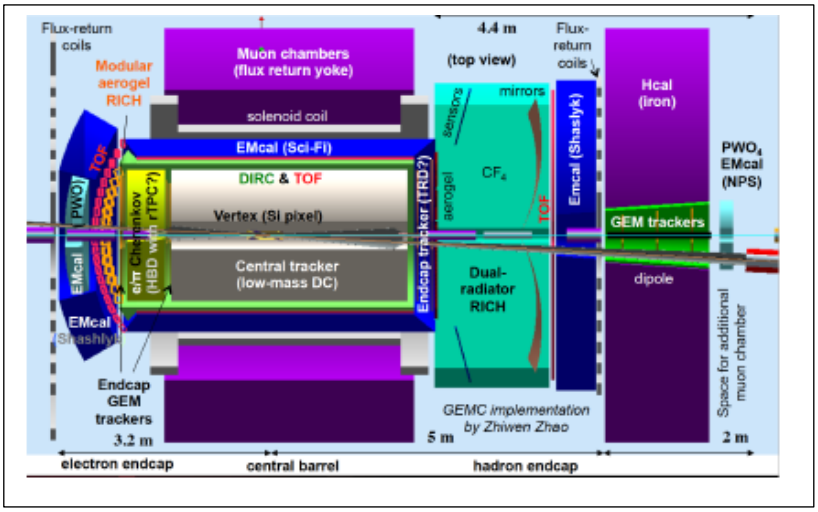

Fig. 2: example layout of the EIC detector

As shown in Fig. 2, the central detector has three regions, backward (electron-going) covering rapidity of -3.5 to -1.0, barrel covering rapidity η= -1.0 to 1.0, and forward (ion-going) covering rapidity of η=1.0 to 3.5. In the electron endcap, particle identification is important for discriminating single photons from, e.g., DVCS and two photons from π^0 decay, and e/p. Resolution is essential for particle reconstruction, which is driven by the need to accurately reconstruct the four-momentum of the scattered electrons at small angles. There, the angular information is provided by the tracker, but the momentum (or energy) can come from either the tracker or the electromagnetic calorimeter. For high electron momenta there will always be a critical angle (rapidity), below which the EM calorimeter will, at high momenta in a solenoidal field, provide the better resolution. Here, this rapidity is η~-2 and required energy resolution is better than $2\%/\sqrt{E}$. At larger angles the requirements of energy resolution may be relaxed to $7\%/\sqrt{E}$. To distinguish photon from proton and to detect high-*x* SIDIS events similar requirements apply in the forward direction. In the barrel a considerably worse energy resolution, $10-12\%/\sqrt{E}$, is allowable. An overview of the requirements is presented in Table 4.

Nomenclature			Tracking			Electrons		HCAL
			Resolution	Allowed X/X_0	Si Vertex	Resolution σ_E/E	PID	Resolution σ_E/E
	Auxiliary Detectors	low-Q2 tagger	$\delta\theta/\theta$<1.5%; $10^{-6}<Q^2<10^{-2}$ GeV^2			TBD		
						TBD		
		Instrumentation to separate charged particles				(1.0-1.5)%/√E+0.5%		
	Central Detector	Backwards Detectors	σ_p/p~-0.1%p+2.0%	~5% or less	TBD		π suppression up to 1:10^4	
			σ_p/p~-0.05%p+1.0%			7%/√E		
		Barrel	σ_p/p~-0.05%p+0.5%		σ_{xyz}~20μm, $d_0(z)$~$d_0(r_\phi)$~$20/p_T$ GeV μm + 5μm	<10%/√E, and likely better		TBD*
		Forward Detectors	σ_p/p~-0.05%p+1.0%		TBD			<35%/√E
			σ_p/p~-0.1%p+2.0%			<2%/√E+1%		
	Auxiliary detectors	Instrumentation to separate charged particles						
		Proton Spectrometer	$\sigma_{intrinsic}$<1%; Acc: $0.2<p_T<1.2$ GeV/c					

Table 4: Overview of EIC detector requirements. [*the exact hadronic calorimetry requirement is under study as a balance of expected particle energy ranges as well as that of missing transverse momentum in charged current events for the EIC energies and the achievable resolutions.]

In summary, the regions and functions of the calorimeters envisioned for the EIC are:

1. ***lepton/backward direction: EM calorimeter*** to detect the scattered lepton with high energy resolution. At rapidities η ~<-2 the energy measurement comes mainly from the calorimeter. The segmentation has to be good enough for particle identification, e.g. to separate proton and photon from DVCS.
2. ***ion/forward direction: EM calorimeter*** to detect high-x SIDIS particles and the electromagnetic part of high-x jets with high resolution
3. ***barrel/mid rapidity: EM calorimeter*** to provide particle identification for leptons in a region where the hadron background is large. These include photons from DVCS, vector mesons, π^0 electromagnetic part of jets
4. ***Hadronic calorimeters*** to measure jet energy

Lepton/Ion Direction *Inner* and *Outer* Endcap EM Calorimeters

The choice of calorimetry at backward rapidity $-4 < \eta < 1$ is driven by the requirement to detect the scattered lepton with high energy resolution, which for rapidity <2, >-2 is determined by the calorimeter alone. Furthermore, the granularity of the calorimeter has to be good enough for particle identification, e.g. to separate proton and photon from DVCS. Calorimetry at forward rapidity $1 < \eta < 3.5$ is driven by the need to identify hadrons produced in semi-inclusive processes, in particular at large x. In both cases, relaxed resolution would be acceptable at larger angles (rapidity).

Fig. 3(left) shows the momentum vs. rapidity distributions in the laboratory frame for photons originating from deeply virtual Compton scattering (DVCS) for different lepton and proton beam energy combinations. For lower lepton energies, photons are scattered in the forward (ion) direction. With increasing lepton energy, photons increasingly populate the central region of the detector. At the highest lepton beam energies, photons are even produced backward (in the lepton-going direction), very close to the electron cluster. Overall, a rapidity coverage of $-4 < \eta < 1$ is needed for DVCS photons. The general patterns of the kinematic distributions of hadrons produced in semi-inclusive processes is shown in Fig. 3(right). A kinematic coverage of $-3.5 < \eta < 3.5$ covers the region in p_T and z that is important to achieve the EIC physics goals, TMD, helicity PDF, FF, asymmetries, cross sections, etc. For imaging studies through exclusive reactions involving light mesons a Q^2 cut must be applied for a valid partonic interpretation. Since exclusive low-Q^2 hadrons are produced in the forward direction, a Q^2>10 GeV2 cut changes the pattern. While the electron is always seen in the electron-going direction, the photon cluster, at low center of mass energies can be produced close to the electron in the electron-going

direction, in the barrel or in the ion-going direction. At larger center of mass energies, the photon is always produced backward in the electron-going direction, very close to the electron cluster.

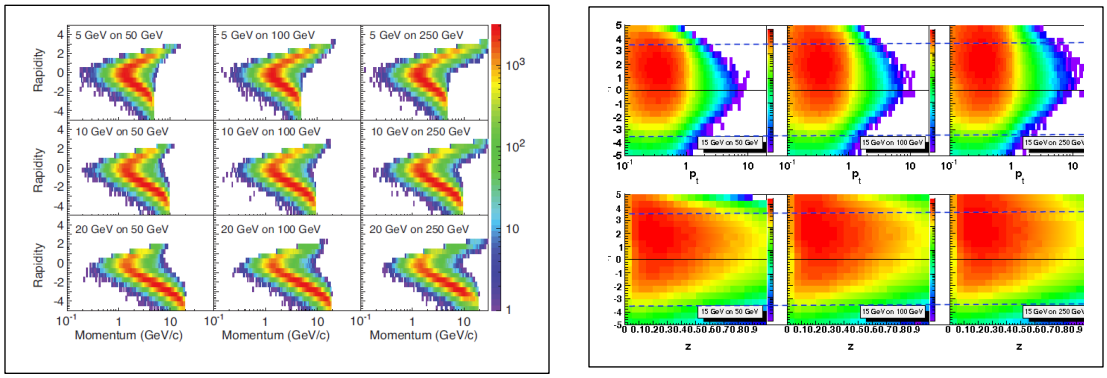

Fig. 3: (left) Energy vs. rapidity for DVCS photons and (right) the SIDIS kinematic coverage for pions with cuts Q^2>1 GeV^2, 0.01 < y < 0.95 and p> 1 GeV

The tracking resolution for a dedicated EIC detector including a barrel silicon tracker and forward silicon trackers (forward GEM, barrel micromegas) is illustrated as a function of rapidity (angle) in Fig. 4. At large absolute values of the rapidity, η,(both forward and backward) the tracking resolution is poor compared with the resolution of $PbWO_4$ crystals (energy resolution better than 3% at room temperature) for all reasonably high energies. For lower magnetic fields the forward tracking resolution would be even lower (gas detector type resolution is ~70 μm vs. while that of silicon is ~20 μm). For comparison, the energy resolution of lead glass is 5-6%. The energy resolution of $PbWO_4$ can be further improved by cooling the crystals.

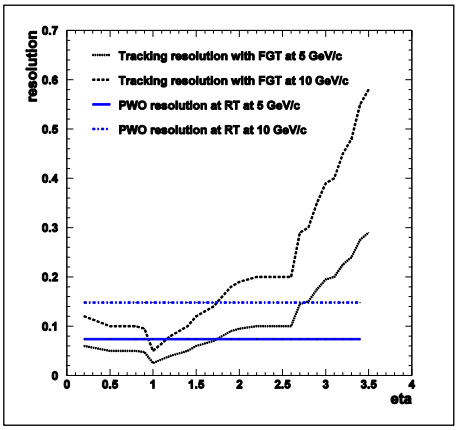

Fig. 4: The resolution as a function of rapidity (eta) for tracker and $PbWO_4$ crystals at representative particle momenta of 5 GeV/c and 10 GeV/c of the experiments. The tracking resolution at large values of eta is relatively poor and can be compensated by that of high resolution crystals

Fig. 5 shows the impact of high-resolution crystal calorimetry at small angles, where the tracking resolution is poor. The quality of the physics measurement is determined to a large extent by the level of bin-to-bin migration in the 2D (x_{bj}, Q^2) kinematic plane. The past experience, in particular the HERMES Collaboration data analysis, indicates that acceptable "bin survival" level (the probability to register the event in the same kinematic bin where it originally occurred), which effectively determines the kinematic reach, should be of on the order of at least 0.6-0.7, spanning from the maximum values of *y* down to the region of $y \sim 0.01$ (where *y* is the DIS variable, describing a fraction of the beam electron energy carried by the virtual photon). A significant fraction of the "small *y*" kinematic domain is characterized by small electron scattering angles and large energy. As discussed above, tracker momentum resolution, which is typically used for the scattered electron track parameter determination, degrades rapidly under these circumstances because of the vanishing effective B*dl integral of the central part of the solenoid field. A crystal calorimeter with the sufficiently high energy resolution in the electron-going direction end-cap can potentially circumvent this problem. Namely the scattered electron momentum can be taken as a weighted mean of the momentum measured by the tracker system and the energy measured by such a calorimeter. A high resolution crystal calorimeter for $\eta<-2$ (PWO crystals) improves the available y range considerably. At rapidity $-2 < \eta < 1$ the resolutions requirement can be relaxed and could be achieved by a sampling calorimeter, e.g. a shashlik or Spacal type. The optimal solution would thus be a combination of an inner (PWO crystal) and outer calorimeter with the following requirements:

The ***inner*** EM endcap calorimeter for rapidity $\eta < -2$ should provide:

1. Good ***resolution in angle*** to at least 1 degree to distinguish between clusters,
2. ***Energy resolution*** to < (1.0-1.5 %/√E+0.5%) for measurements of the cluster energy,
3. ***Time resolution*** to < 2ns
4. Cluster threshold: 10 MeV
5. Ability to withstand radiation down to at least 1 degree with respect to the beam line.

The ***outer*** EM endcap calorimeter for rapidity $-2 < \eta < 1$ should provide:

1. ***Energy resolution*** to 7%/√E for measurements of the cluster energy,
2. ***Compact readout*** without degrading energy resolution
3. ***Readout segmentation*** depending on angle

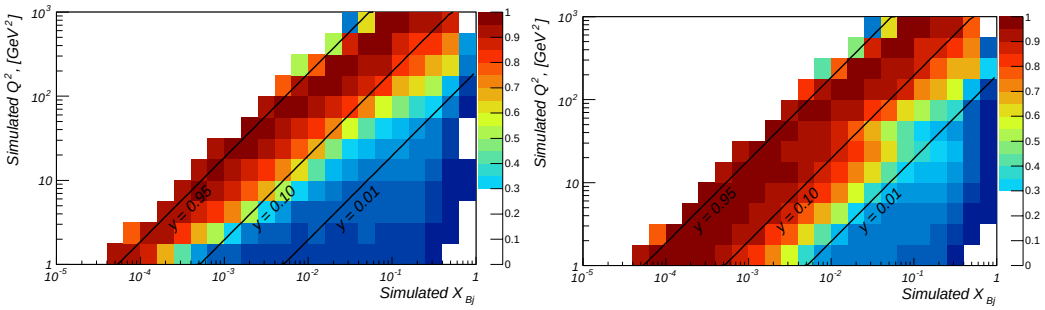

Fig. 5: Inclusive DIS event parameter migration in the {x_{bj}, Q^2} kinematic plane. Pythia 20x250GeV events, external bremsstrahlung turned off. Only the area with survival probability >0.6-0.7 is suitable for the

conclusive analysis. Left panel: only the tracker information is used to calculate scattered electron momentum. Right panel: same events, but a weighted mean of the tracker momentum and the crystal calorimeter energy is used. Calorimeter resolution is taken to be $\sigma_E/E \sim 2.0\%/\sqrt{E}$ for pseudo-rapidities below -2.0 and $\sim 7.0\%/\sqrt{E}$ for the rest of the acceptance.

To make a clear positive impact on the scattered electron kinematics determination, a crystal calorimeter ($PbWO_4$) in the electron-going end-cap direction should have a constant term of at most ~0.5%, while a stochastic term on the order of 1.0-1.5% would suffice. This is illustrated in Fig. 6.

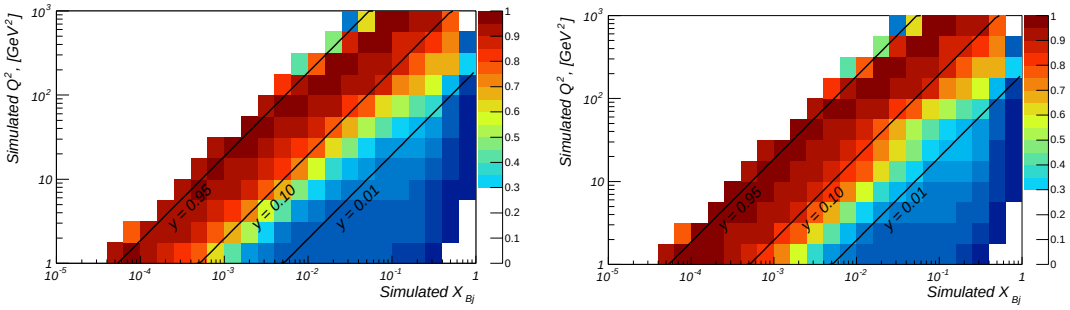

Figure 6. Same set of events as in Fig.5. Weighted mean of the tracker momentum and the crystal calorimeter energy is used. Left panel: calorimeter resolution is taken to be $\sigma_E/E \sim 1.75\%/\sqrt{E} + 1.15\%$ (PrimEx PWO calorimeter at JLAB [1]) for pseudo-rapidity below -2.0 and $\sim 7.0\%/\sqrt{E}$ for the rest of the acceptance. Right panel: "ideal" calorimeter resolution $\sigma_E/E \sim 1.0\%/\sqrt{E} + 0.5\%$ for $\eta<-2$.

Barrel EM Calorimeters

The choice of calorimetry at central rapidity is driven by the need to provide particle identification in a region where the hadron background is large. Measuring the ratio of the energy and momentum of the scattered lepton, typically gives a reduction factor of ~100 for hadrons. In this region the energy measurement can be supplemented by tracking detectors, and thus noticeably worse energy resolution of the calorimeter suffices.

Fig. 7 shows the momentum distribution for the scattered lepton for different rapidity bins and three different lepton-proton beam energy combinations.

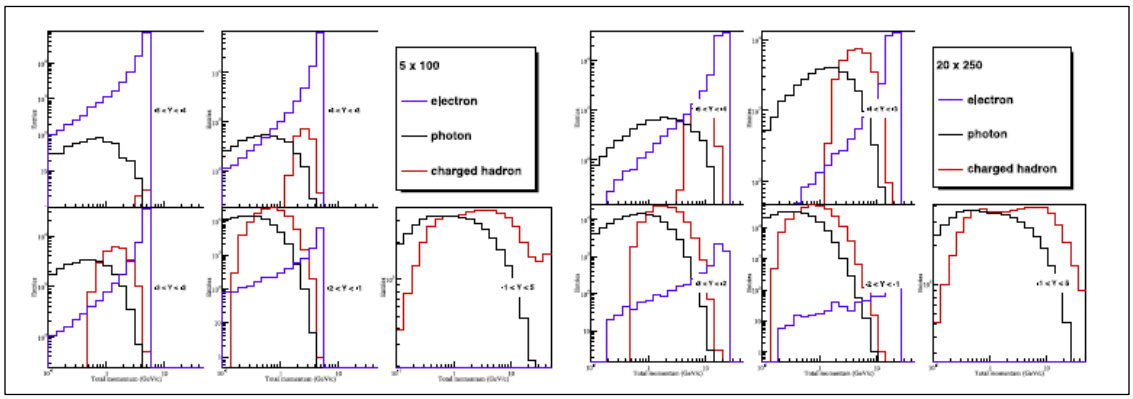

Fig. 7: Distribution of the total momentum for electrons, photons and hadrons.

The $Q^2 < 10$ GeV^2 events typically correspond to negative rapidity ($\eta < -3$) and $Q^2 > 10$ GeV^2 correspond to rapidity $\eta > -2$ for 5 GeV x 50 GeV and $\eta > -2$ for 30 GeV x 50 GeV. Depending on the center-of-mass energy the rapidity distributions for hadrons (both charged and neutral) and the scattered lepton overlap and need to be disentangled. The kinematic region in rapidity over which hadrons and photons need to be suppressed with respect to electrons depends on the center-of-mass energy. For lower center-of-mass energies, electron, photon and charged hadron rates are roughly comparable at 1 GeV/c total momentum and $\eta = -3$. For the higher center-of-mass energy, electron rates are a factor of 10-100 smaller than photon and charged hadron rates, and comparable again at a 10 GeV/c total momentum (See Fig. 7.18 in Ref.~\cite{Boer:2011fh}). This adds another requirement to the detector: good electron identification. The kinematic region in rapidity over which hadrons and also photons need to be suppressed, typically by a factor of 10 - 100, shifts to more negative rapidity with increasing center-of-mass energy.

To satisfy the Particle Identification (PID) requirements in the barrel, EM calorimetry should provide:

1. ***Compact design*** as space is limited
2. ***Energy resolution*** to < (10-12%/√E) for leptons in a region where the hadron background is large
3. ***No need for 2D projectivity***
4.

Hadron calorimetry

The requirement on hadron calorimetry comes from requirements on jet energy resolution and linearity in the hadron-going direction. For the LHC physics program the jet energy resolution requirements is $\sim 50\%/\sqrt{E}$ *+3%*. This can be achieved with a hadronic resolution of ~ $42\%/\sqrt{E}$. Hadronic calorimetry at EIC in the forward region, $1 < \eta < 4$ with a stochastic term of the hadronic energy resolution of $50\%/\sqrt{E}$ seems sufficient for accessing gluon polarization using dijets to tag photon-gluon fusion events. These studies require the highest energies ($\sqrt{s}$=141 GeV) and luminosity to accumulate statistics at high p_T. The dominant contribution to jet energy resolution at these high energies comes from the constant term, which includes nonlinearities. For studies at low p_T requiring sufficient resolution at large x for accessing inclusive jet cross-sections in DIS, the stochastic term becomes important. For optimal resolution for jet identification, a hadronic energy resolution of better than that achieved at ZEUS (35%/√E) combined with low EM energy resolution would be preferable. At HERA, uncertainties at low

and medium values of Q2 were dominated by the jet energy scale uncertainties, which were on the order of 1-2% and translated into 5-10% uncertainties in the cross section.

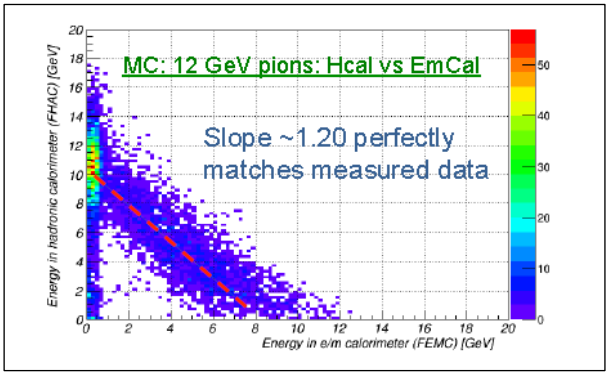

Fig. 8: Example of energy in hadronic and electromagnetic calorimeters.

To satisfy this requirement, particle identification in the hadron endcap should provide:

1. ***Hadron energy resolution*** to < 35%/√E,
2. ***EM energy resolution*** *to* < (2%/√E + 1%)
3. ***Jet energy resolution*** < (50%/√E + 3%)
4. ***No need for hadron calorimeter at mid-rapidity (in barrel) as have tracker there***

References

1. M. Kubantsev, "Performance of the PrimEx electromagnetic calorimeter", AIP Conf. Proc. 867 (2006) 51
2. A. Alavi-Harati et al., Phys. Rev. Lett. 83 (1999) 22
3. V. Prasad, "Performance of the cesium iodide calorimeter at the KTeV experiment at Fermilab", Nucl. Inst. Meth. A 461 (2001) 341
4. D. Boutigny et al., The BaBar Technical Design Report (SLAC-R-457)
5. B. Lewandowski, "The BaBar electromagnetic calorimeter", Nucl. Inst. Meth. A 494 (2002) 303
6. A. Abashian et al., Nucl. Inst. Meth. A 479 (2002) 117
7. Y. Oshima et al., "Beam test of the CsI(Tl) calorimeter for the Belle detector at the KEK-B factory, Nucl. Inst. Meth. A 380 (1996) 517
8. CMS Collaboration, The Electromagnetic Calorimeter Project Technical Design Report (CERN/LHCC/97-33)
9. M. Aleksa, M. Diemoz, "Discussion on the electromagnetic calorimeters of ATLAS and CMS", Nucl. Inst. Meth. A 732 (2013) 442.
10. J.A. Bakken et al., Nucl. Inst. Meth. A 228 (1985) 296
11. R. L. Sumner et al., "The L3 BGO Electromagnetic Calorimeter", Nucl. Inst. Meth. A 265 (1988) 252.
12. C. Bebek et al., Nucl. Inst. Meth. A 265 (1988) 258

13. M. Akrawy et al., Nucl. Inst. Meth. A 290 (1990) 76
14. G.D. Barr et al., CERN/SPSC/90-22, SPSC/P253 (1990)
15. V. Fanti et al., Phys. Lett. B 465 (1999) 335
16. U. Behrens et al., Nucl. Inst. Meth. A 289 (1990) 115
17. L. Balka et al., Nucl. Inst. Meth. A 67 (1988) 272
18. M. Adinolfi et al., Nucl. Inst. Meth. A 482 (2002) 363
19. A. Antonelli et al., Nucl. Inst. Meth. A 354 (1995) 352
20. A. Decamp et al., Nucl. Inst. Meth. A 294 (1990) 121
21. M. Derrick et al., Nucl. Inst. Meth. A 309 (1991) 77
22. B. Aubert et al., Liquid Argon Calorimetry with LHC Performance Specifications (CERN/DRDC/90-31)
23. S. Lee et al. "Hadron Detection with a dual-readout fiber calorimeter", arXiv:1703:09120v1 (2017)
24. A. Accardi et al., "Electron-Ion Collider: The Next QCD Frontier – understanding the glue that binds us all", Eur.Phys.J. **A52** (2016) no.9, 268**,** arXiv.1212.1701, BNL-98815-2012, JLAB-PHY-12-1652 (2012)
25. D. Boer et al., "Gluons and the sea quarks at high energies", arXiv.1108.1713, BNL-96164-2011, JLAB-PHY-11-1373 (2011)
26. S. Abeyratne et al., "Science Requirements and Conceptual Design for a Polarized Medium Energy Electron-Ion Collider at Jefferson Lab", arXiv.1209.0775 (2012).